ISSN No. 2454-6194 | DOI: 10.51584/IJRIAS | Volume VIII Issue VII July 2023

Effect of Blade Number on the Performance of a Centrifugal Pump Using Commercial Tool ANYS 91.2

Daniel-Kyei Kankam[1], Castro Owusu- Manu Kwabena[2], Dominic Boateng[3], Alexander Fordjour[4*]

[1]*Takoradi Technical University, Faculty of Engineering, Takoradi, Western Region, Ghana*

[2]*Ho Technical University, Faculty of Engineering, Ho, Volta Region, Ghana*

[3]*Faculty of Engineering and Technology, Department of Mechanical Engineering, Kumasi Technical University, Kumasi, Ashanti Region, Ghana*

[4]*Koforidua Technical University, Faculty of Engineering, Koforidua- Eastern Region, Ghana*

**Correspondence Author*

DOI: https://doi.org/10.51584/IJRIAS.2023.8710

Received: 31 May 2023; Revised: 18 June 2023; Accepted: 27 June 2023; Published: 03 August 2023

Abstract: Computational fluid dynamics (CFD) is frequently used in centrifugal pump design. The characteristics of the flow fields around turbomachinery can be simulated using tools for numerical computational fluid dynamics in three dimensions. Numerical simulation, which also provides significant information for the hydraulic design of the centrifugal pump, can be used to visualize the internal flow condition of a centrifugal pump. The purpose of this study was to examine the effect of blade number on the hydraulic performance curve using a commercial instrument. ANSYS 91.2. code commercial.The geometric model of the pump was built using CF turbo, and the flow domain was meshed using the commercial programme ICEM. The results demonstrated that an increase in the number of blades significantly improved the hydraulic performance of the centrifugal pump's head. The findings also revealed that the area of the low-pressure zone at the blade's input suction grew and that the static pressure distribution homogeneity in the diffusion section was significantly better than that in the spiral section. The design flow of 35 m3 per hour is where the best efficiency point (BEP) is located. At Z = 6 and Z = 7, the head values were 51.58 m and 53.13 m, respectively, while the efficiency values were 50.32% and 53.35%. The comparison of the H-Q curve for estimated head discharge indicates that all impeller efficiency curves share the same fundamental tendency.

Keywords: Impeller; Blade number; Centrifugal pump; Hydraulic efficiency

I. Introduction

In recent years, numerical simulation technology has developed as one of the most effective and economical methods for analyzing the flow inside the pump and predicting its characteristics. Centrifugal pumps are among the most extensively used pieces of machinery in a range of applications, including industry, residences, power plants, agriculture, water supply, and transportation, according to Asuaje et al. (2005), Shah et al. (2013), and Usha et al. (2010). The centrifugal pump works on the forced vortex concept. The prime mover (electrical energy) is converted into kinetic energy and pressure energy by the pump's two main parts, the impeller and volute. These pumps must function well due to the wide range of applications for centrifugal pumps, which rely on blade characteristics such as blade inlet, blade number, and outlet angle and are governed by the speed triangle. A centrifugal pump uses hydrodynamic energy, which is created when the rotating kinetic energy of the fluid flow is transferred into the fluid flow. An impeller is used to move the fluids from an area of low pressure (the inlet) to an area of higher pressure (the output). The fluid is forced toward the pump by air pressure because centrifugal pumps create negative pressure at the inlet pressure (Supponen et al. 2018; Ghorbani et al. 2015). The characteristics of the centrifugal pump impeller blade have a considerable impact on the pump head and efficiency. The effect of the blade trailing edge angle on centrifugal pump performance has been the subject of theoretical and experimental research by certain scientists. Bacharoudis et al.2008 looked at how three trailing edge angles—20, 30, and 50—affected the capacity to maintain a consistent diameter. It was found that the hydraulic efficiency rose with increasing oil but fell with increasing water as the working medium. The head of water and oil increased with an increase in blade outlet angle. The numerical results' trend and the experiment's findings are strongly congruent. The results show that the outlet angle is greater than 32.50 for 90 outlet angles. Gonzalez et al. (2006) studied the radial thrust on a single-blade centrifugal impeller with two different blade outlet angles using experiment and numerical simulation. Liu et al. 2001 also looked at rotors in micro turbopumps with three different output angles. According to (Liu et al. 2014; Stavropoulos et al. 2021) the trailing edge of the blade will have an effect on the vortex intensity and vortex shedding frequency. Additionally, Zobeiri et al. 2012 looked studied the effect of an inclined blade's trailing edge on vibration brought on by vortices. Numerous studies on centrifugal pumps optimized the geometric

ISSN No. 2454-6194 | DOI: 10.51584/IJRIAS | Volume VIII Issue VII July 2023

parameters of the pump while also controlling and reducing the amount of pressure pulsation. Spence and Aaral 2009 performed a numerical analysis of the effects of geometric features such as tip clearance, blade arrangement, and clearance on the pressure pulsation of centrifugal pumps. According to a study by Yang et al. (2014), increasing the space between the impeller and volute will decrease pump efficiency by reducing the magnitude of pressure pulsation. In this study, the impact of blade number on the hydraulic efficiency of centrifugal pumps is investigated using the commercial tool ANYS 91.2.

Geometric model and meshing generation

The centrifugal pump used in this study has a 50 m3/h rated flow, 45 m rated head, and 2900 rpm rated speed. The major elements and design parameters for the pump are listed in Table 1. Figure 1 shows how a commercial CF turbo was used to build the geometric model of the pump.

Figure 1: Geometric model of the centrifugal pump

The intake and exit of the pump were appropriately enlarged to reduce the influence of boundary conditions on internal flow. As shown in Figure 2, the convective field was created using the premium program ICEM. Grids for the impeller and volute are tetrahedral whereas those for the suction pipe are hexahedral. The mesh independence of the geometric model was established to reduce calculation times and ensure calculation precision. When the number of grids was increased from 666514 to 1448920, the simulated head and efficiency slightly improved. There were only slight changes in the head and efficiency, less than 0.4%, from 1,448,920 to 2,012,537 grids. The intake pipe and suction pipe, 476,161 grids of the impeller, 73,9651 grids of the volute, and 19,000 grids of the outlet pipe make up the total number of grids in the geometric model utilized in the simulation, which is 1,448,920.

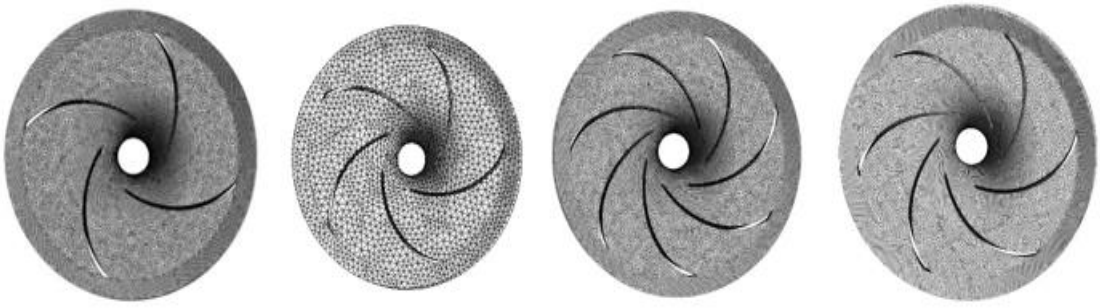

Figure 2. The grids of the impeller for different blade numbers, Z=4 ,Z=5, Z=6, and Z=6 Z=7

ISSN No. 2454-6194 | DOI: 10.51584/IJRIAS | Volume VIII Issue VII July 2023

Table 1: Pump features and dimensions

S/n	Description of feature	Notation	Size
1	Suction pipe diameter	(D_s/mm)	25
2	Pump outlet diameter	(D_{out}/mm)	70
3	Blade outlet width	(b_2/mm)	12
4	Blade number	(Z)	4-7
5	Blade outlet diameter	(D_2/mm)	208
6	Blade inlet angle	(β_{1y}%)	22
7	Blade outlet angle	(β_{2y}%)	24
8	Tongue angle	(φ%)	19
9	Volute inlet width	(b_3/mm)	24
10	Base circle diameter	(D_3/mm)	218

Boundary conditions and initialization

The no-slip condition was maintained on the wet walls. At the inlet of the suction pipe, there is only a uniform axial velocity, which can be determined by a given flow rate and the inner diameter of the suction pipe. In the impeller, the boundary conditions must be specified correctly to obtain the exact solution. For this study, all simulations were carried out in the steady-state model. The convergence criteria were taken as 1000 for all the cases. The impeller domain of the centrifugal pump is regarded as a rotating frame. Water was taken as continuous fluid at ambient temperature (25°C) and the inlet and outlet of the pressure were set as 1atm. To complete the numerical simulation, the time step was set as follows: The Centrifugal pump impeller domain is considered a rotating frame. $Timestep = \frac{4}{2900 \times 90}$ 0.00023 s representing 4° of each impeller rotation. The impeller is set to eight complete revolutions with a total time of 0.0864 s. Considering the accuracy, 10 maximum coefficient convergence control loops were selected in each time step, and the simulation time step is set to 0.0003s.

II. Mathematical Model.

Governing equations and turbulence model

In this paper. Reynolds time-averaged Naiver-Stokes equation (RANS) was used for the numerical simulation (Asuaje et al. 2008; Liu et al. 2001; Yu et al. (2000). The main form of N-S equations is as follows.

The continuity equation is

$$\frac{\partial p_{mix}}{\partial t} + \frac{\partial(\rho_{mix} u_i)}{\partial x_i} \qquad (1)$$

The momentum equation is

$$\frac{\partial p_{mix}}{\partial t} + \frac{\partial(\rho_{mix} u_i u_j)}{\partial x_i} = -\frac{\partial p}{\partial x_i} + \frac{\partial}{\partial x_j}\left(u \frac{\partial u_i}{\partial x_j}\right) + \frac{\partial \tau_{ij}}{\partial x_j} \qquad (2)$$

Where ρ and u are the pressure and time-averaged velocity, respectively. μ is the fluid dynamic viscosity = - ρ u'u' is the Reynolds stress, and is the density of the mixture. Where n represents the number of phases, and a is the volume fraction. In this paper, the media pumped gas and liquid. Hence, the number of phases n is 2. Because the SST k-□, turbulence model takes into account the transfer of turbulent shear stress more accurate results can be obtained in the near-wall region, and the flow separation can be well, Therefore, the SST k-□, a turbulence model is suitable for predicting the performance of the pump studied in this paper.

The equations of this turbulence model are as follows:

$$\frac{\partial(pk)}{\partial t} + \frac{\partial(pku_i)}{\partial x_i} = \frac{\partial}{\partial x_j}\left(\Gamma_k \frac{\partial k}{\partial x_j}\right) + G_k - Y_k + S_k \qquad (3)$$

ISSN No. 2454-6194 | DOI: 10.51584/IJRIAS | Volume VIII Issue VII July 2023

$$\frac{\partial(p\square)}{\partial t} + \frac{\partial(p\square u_i)}{\partial x_i} = \frac{\partial}{\partial x_j}(\Gamma_\square \frac{\partial \square}{\partial x_j}) + G_\square - Y_\square + D_\square + S_\square \quad (4)$$

$$\mu = \rho \frac{k}{\omega} \quad (5)$$

where ρ is the density. Γk and Γ□ are the effective diffusion coefficients of turbulent kinetic energy k and dissipation frequency □, respectively, Gk is the source term of turbulent kinetic energy k. G□ is the source term of dissipation frequency □. Yk and Y□ are the diffusions of turbulent kinetic energy k and dissipation frequency of, respectively. D□ is the cross-diffusion term. Sk and S□ are the source terms defined by users. and μi, is the turbulent viscosity

III. Results and Discussions

The pressure distribution for different blade numbers—4, 5, 6, and 7—is shown in Figure 3. Figure 3 shows how, for different numbers of blades, the static pressure gradually increases as it leaves the impeller at the outlet. For an impeller with the same radius, the static pressure on the pressure side is greater than the static pressure on the suction side. The static pressure at the volute outlet increases as the number of blades increases, the static pressure distribution in the spiral section becomes more unstable, and the static pressure distribution in the diffusion section steadily improves. A distinct low-pressure zone with varying numbers of blades is present on the impeller on the suction side of the blade inlet. Therefore, this transition flow pattern may emerge inside the impeller blade and its blade channel as well as inside the pump pipe when the inlet flow is uneven. The surface flow pressure zone's expansion shows how the number of blades has a substantial impact on the pump's characteristics. The total pressure at the outside circumference rises as the blade angle increases while the negative pressure at the inlet decreases. These two pressures work together to improve the impeller's net pressure as well as the blade outlet angle. The friction loss of the bearing and the friction of the impeller disc are to blame for this phenomena.

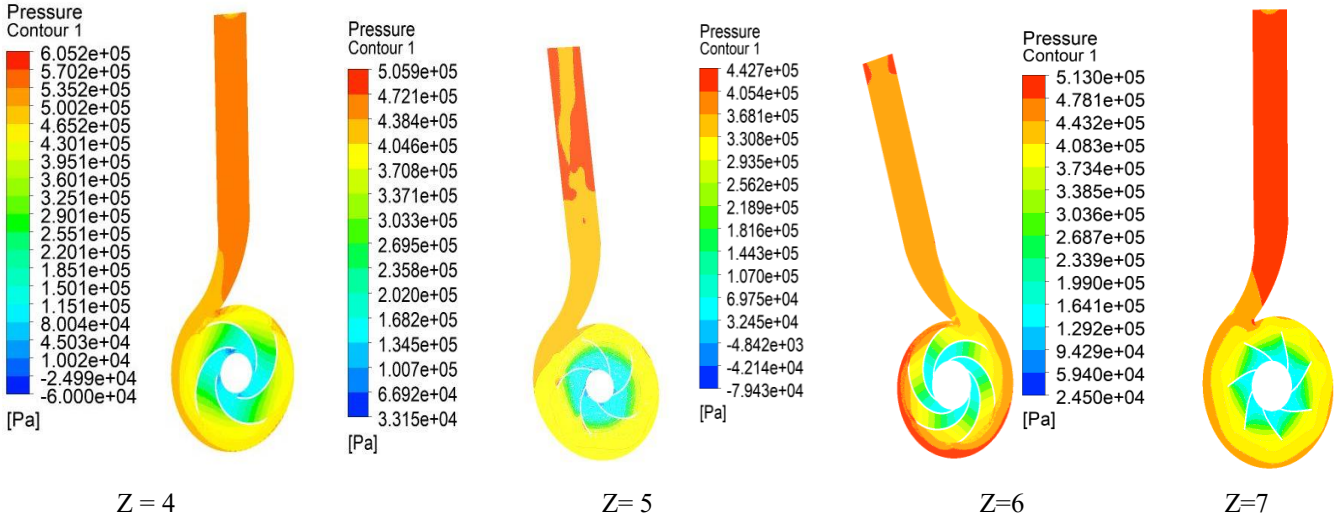

Z = 4 Z= 5 Z=6 Z=7

Figure 4: Pressure distribution for different blade numbers, Z = 4, Z= 5, Z=6 and Z = 7.

Velocity distribution for different blade numbers

The four successive maps in Figure 4 unambiguously depict how a blade passes through the tongue of a volute and how an impeller engages with a volute. When one particular blade goes toward and away from the tongue, there are perceptible velocity variations in that region. When compared to the downstream portion of the volute screw section, where velocity continuously increases from the volute tongue to the outlet along the flow direction, the velocity gradient at the volute tongue is larger. The time-varying velocity is clearly visible close to the monitoring locations Z=6 and Z=7, but nearly unchanged at the screw section. Figure 4 depicts a similar propensity for streamlining variation near points Z=4 and Z=5. The relative velocities of the internal impeller are shown in Figure 4. On the suction side of the trailing edge, we can see the separation trend even if the flow velocity is lower than the nominal one. The absolute velocity vectors near the tongue with a flow rate larger than the nominal are shown in Figure 4. Here, it is clear that there is an obstruction between the tongue and the impeller as well as a separation on the output side.

ISSN No. 2454-6194 | DOI: 10.51584/IJRIAS | Volume VIII Issue VII July 2023

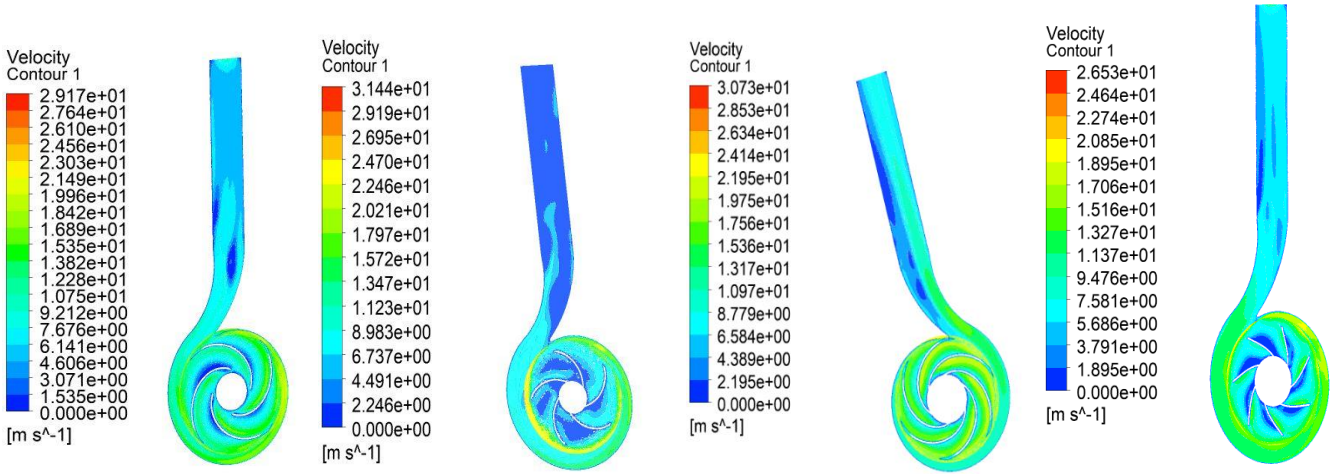

Z= 4 Z= 5 Z=6 Z= 7

Figure 4: Velocity distribution for different blade numbers, Z = 4, Z= 5, Z=6 and Z = 7.

Analysis of turbulent kinetic energy

Figure 5 displays the distribution of turbulent kinetic energy for various blade counts. The present computation results have a maximum value of 12 m2/s2 and a lowest value of 0.2 m2/s2. Figure 5 shows that the turbulence intensity amplitude is lowest close to the pump's inlet and volute at about the same time. All of these unfair results are the result of the volute tongue shape. All of these asymmetric results can be attributed to the influence of the volute tongue structure. Figure 5 illustrates the clearly high turbulent kinetic energy position on the back of the blade inlet. This proves that there is both a sizable amount of turbulent kinetic energy near to the third zone where the blade hits the impeller as well as a certain impact energy loss in the liquid of the blade. This is due to the substantial energy losses caused by both fluid flow and blade impact. The fluid has no effect on the solid wall or the impeller exit, and the impeller outlet has very little turbulent kinetic energy. This is somewhat in line with the impeller's maximum diameter design concept. Additionally, as the number of blades grows, the turbulent kinetic energy gradually increases. It becomes clearer at Z = 6 mm. Therefore, to maximize the pump's operational effectiveness under design parameters, the blade thickness should fall within a specific range.

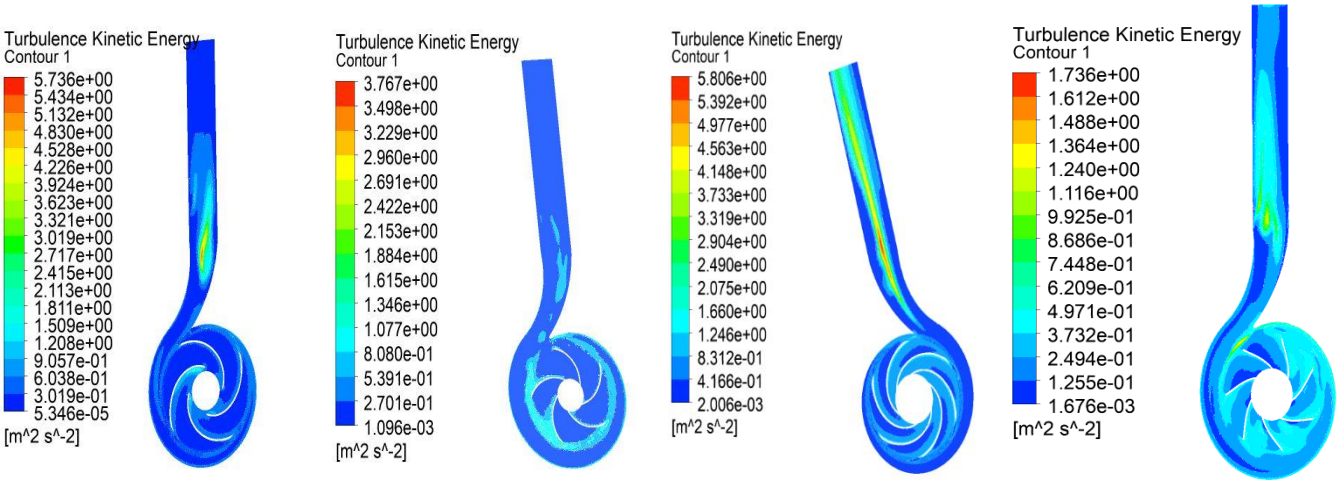

Z= 4 Z=5 Z=6 Z=7

Figure 5: The distribution of turbulent KE for different blade numbers, Z=4,Z= 5,Z=6 and Z = 7

Performance characteristic curve

The pump performance curve is depicted in Figure 6 with varying numbers of blades. Figure 6 illustrates how the flow affects the head, power input to the pump shaft, and pump efficiency as the flow increases. All blades reach their peak heads and efficiency before beginning to lose some of it. The relationship between power and discharge shows that power grows with the number of

ISSN No. 2454-6194 | DOI: 10.51584/IJRIAS | Volume VIII Issue VII July 2023

blades. These results are in line with those of past studies using other parameters (Wang et al. 2018; Sun et al. 2016; Guo et al., 2017; Wang et al. 2023). When the number of blades increased from 4 to 7, there was a growth of approximately 3.47%. Because the tangential component of torque increases with the number of blades, the power also increases with the number of blades because the torque transmitted to the blades increases. The increased output power, head, and efficiency of the impeller with an increase in the number of blades can be attributed to the pump casing. At high flow rates, the number of blades will improve hydraulic efficiency. With efficiency values of 50.32% and 53.35%, and head values of 51.58 m and 53.13 m for blade numbers Z = 6 and Z = 7, respectively, the best efficiency point (BEP) is at a design flow of 35 m3 per hour.

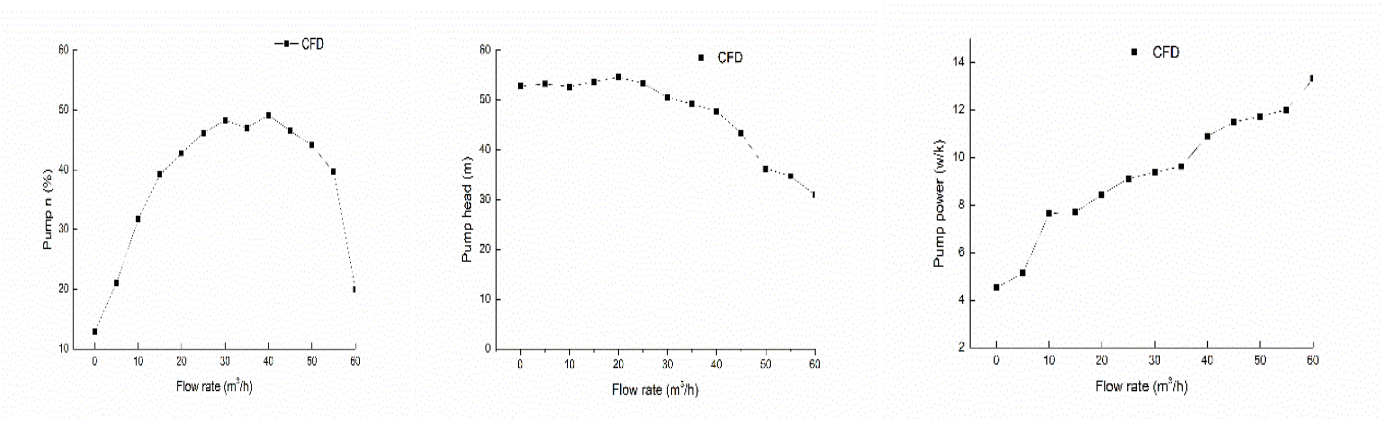

Z=4

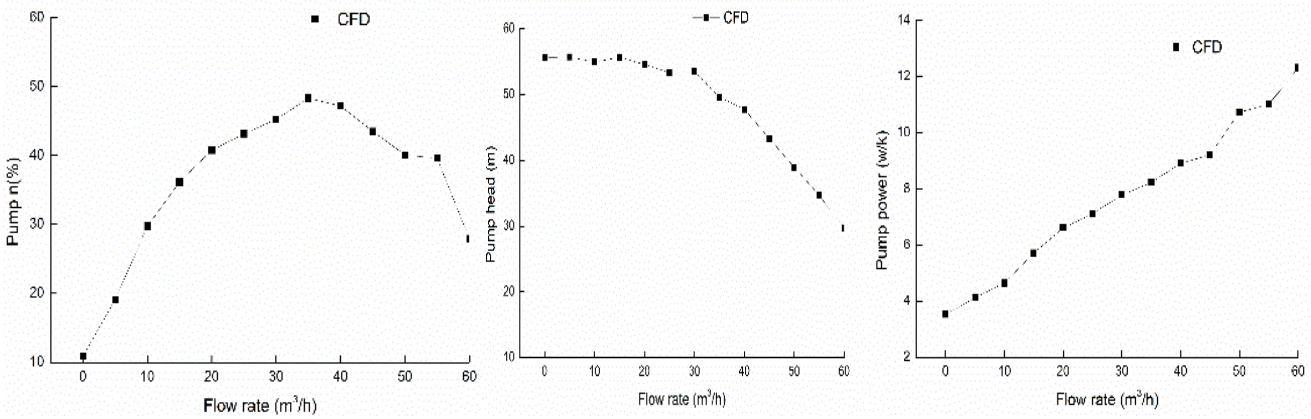

Z=5

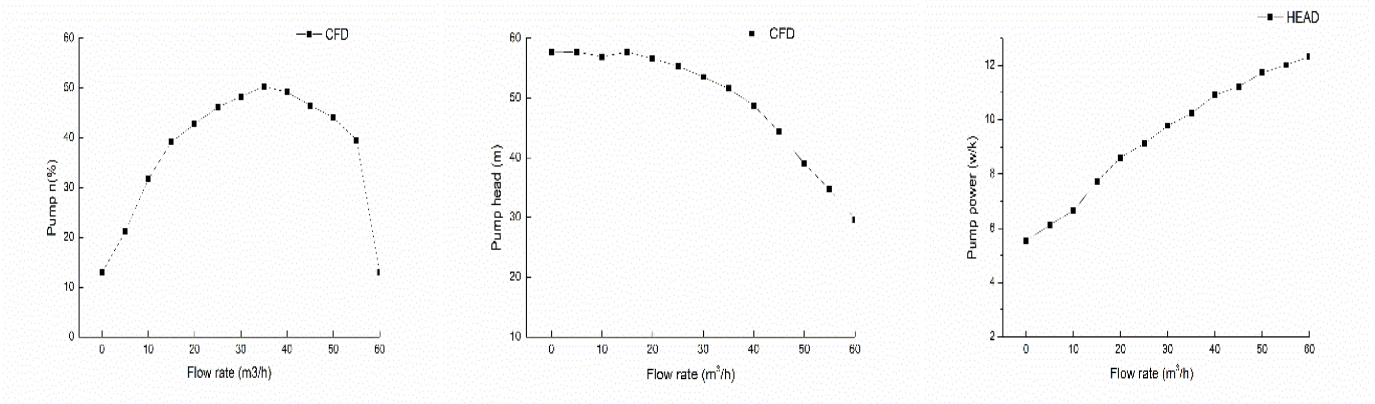

Z=6

ISSN No. 2454-6194 | DOI: 10.51584/IJRIAS | Volume VIII Issue VII July 2023

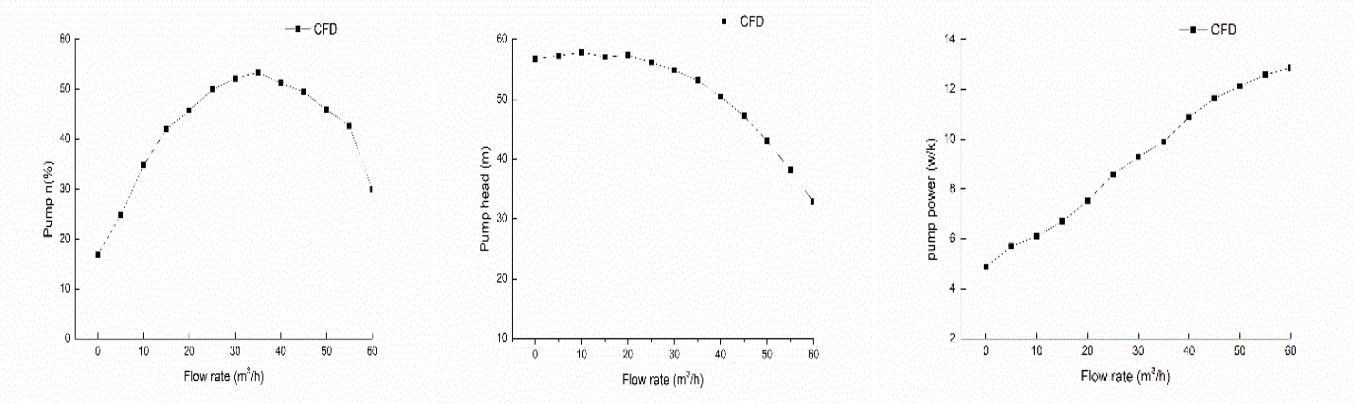

Z=7

Figure 6: Pump performance curve for different blade numbers.

IV. Conclusions

This article describes the numerical simulation of a centrifugal pump using the industry-standard features of ANSYS software. The recent research makes it evident that computational fluid dynamics is an essential and useful tool for pump designers. These conclusions are supported by this study: The hydraulic performance of the centrifugal pump's head has been greatly enhanced with the addition of blades. The findings also showed that the area of the low-pressure zone at the blade's inlet suction grows and that the spiral section's static pressure distribution uniformity deteriorates over time while the diffusion section's static pressure distribution improves. The design flow of 35 m3 per hour is where the best efficiency point (BEP) is located. At Z = 6 and Z = 7, the head values were 51.58 m and 53.13 m, respectively, while the efficiency values were 50.32% and 53.35%. All impeller efficiency curves exhibit the same overarching tendency, according to the comparison of the predicted head discharge H-Q curve.

Reference

1. Asuaje, M., Bakir, F.& Kouidri S., Numerical modelization of the flow in centrifugal pump: volute influence in velocity and pressure fields. Int J Rotat Mach. 3: 244–255,2005
2. Asuaje J., M.,Kenyery, F.,Tremante, A.& Aguillon, O.,Characterization of a Centrifugal Pump Impeller under Two-Phase Flow Conditions. Journal of Petroleum Science and Engineering. 63,p. 18,2008.
3. Bacharoudis, E., Filios A., Mentzos, M.&Margaris D.,Parametric Study of a Centrifugal Pump Impeller by Varying the Outlet Blade Angle. The Open Mechanical Engineering Journal 2, p. 75,2008.
4. Gonzalez, J., Parrondo, J.& Santolaria C., Steady and unsteady radial forces for a centrifugal pump with impeller to tongue gap variation. ASME J Fluids Eng. 128: 454–462,2006.
5. Guo, Y. Study on the Non-Constant Characteristics of Centrifugal Pump Torque and Speed; Jiangsu University: Zhenjiang, China, 2017.
6. Ghorbani, M.; Alcan, G.; Yilmaz, D.; Unel, M.; Kosar, A. Visualization and image processing of spray structure under the effect of cavitation phenomenon. J. Phys. Conf. 2015, 656, 012115.
7. Liu S.,Michihiro N. &Yoshida K., Impeller Geometry Suitable for Mini Turbo-Pump. Journal of Fluids Engineering 123, p. 500,2001.
8. Liu, H.; Wang, J.; Wang, Y.; Zhang, H.; Huang, H. Influence of the Empirical Coefficients of Cavitation Model on Predicting Cavitating Flow in Centrifugal Pump. Nav. Archit. Ocean Eng. 2014, 6, 119–131
9. Shah S. R., Jain S. V., Patel R. N.& Lakhera V.J., CFD for Centrifugal pumps: a review of the state-of-the-art. Journal of ELSEVIER. 715-720,2013.
10. Spence, R. & Aaral-Teixeira J., A CFD Parametric Study of Geometrical Variations on the Pressure Pulsations and Performance Characteristics of a Centrifugal Pump. Comput. Fluids. 38: 1243–1257,2009.
11. Stavropoulos-Vasilakis, E.; Kyriazis, N.; Jadidbonab, H.; Koukouvinis, P.; Gavaises, M. Review of Numerical Methodologies for Modeling Cavitation. Cavitation Bubble Dyn. 2021, 1–35.
12. Supponen, O.; Farhat, M.; Obreschkow, D. High-speed imaging of high pressures produced by cavitation bubbles. In Proceedings of the International Conference on High-Speed Imaging and Photonics 2018, Enschede, The Netherlands, 8–12 October 2018.
13. Sun, H.; Yuan, S.; Luo, Y.; Guo, Y. Analysis of non-constant flow inside a centrifugal pump with the joint action of water and electricity. J. Drain. Irrig. Mach. Eng. 2016, 34, 122–127,150.

ISSN No. 2454-6194 | DOI: 10.51584/IJRIAS | Volume VIII Issue VII July 2023

14. Usha P., Syamsundar C.2010. Computational analysis on performance of a centrifugal pump Proceedings of the 37th National &4th International Conference on Fluid Mechanics and Fluid Power. Chennai, India, paper#TM-07.
15. Yu S., N. G, B., Chan, W.& Chua, L., The Flow Patterns within the Impeller Passages of a Centrifugal Blood Pump Model. Medical Engineering & Physics 22, p. 381,2000.
16. Wang, J.; Wang, Y.; Liu, H. Rotating Corrected-Based Cavitation Model for a Centrifugal Pump. J. Fluids Eng. 2018, 140, 111301.
17. Wang, J.; Sun, L.; Zhou, Y.; Liu, Y.; Zhao, F. Numerical Simulation of Cavitation Characteristics of a Centrifugal Pump Based on an Improved ZGB Model. Processes 2023, 11, 438. https://doi.org/10.3390/pr11020438
18. Zobeiri A., Ausoni P., Avellan, F.& Farhat M., How Oblique Trailing Edge of a Hydrofoil Reduces the Vortex-Induced Vibration," J. Fluids Struct. 32: 78–89,2012.